RSC Advances

PAPER

View Article Online
View Journal | View Issue

Cite this: *RSC Adv.*, 2021, **11**, 24949

Development of a cyan blue-emitting $Ba_3La_2(BO_3)_4$:Ce^{3+},Tb^{3+} phosphor for use in dental glazing materials: color tunable emission and energy transfer†

Gyu Jin Jeong,[ab] Tae Wook Kang,*[a] Young Ji Park,[a] Ye Jin Park,[ac] Younki Lee,[b] Byungseo Bae*[d] and Sun Woog Kim *[a]

Received 7th June 2021
Accepted 8th July 2021

DOI: 10.1039/d1ra04384f

rsc.li/rsc-advances

The Ce^{3+}/Tb^{3+} doped $Ba_3La_2(BO_3)_4$ phosphors were synthesized by a conventional solid state reaction method. The synthesized phosphor samples are a single phase of $Ba_3La_2(BO_3)_4$ and showed angular-shaped fine grains with average particle size from 5 μm to 10 μm. The $Ba_3La_2(BO_3)_4$:Ce^{3+} phosphors showed an asymmetric broad blue emission under excitation at 365 nm and the $Ba_3La_2(BO_3)_4$:Tb^{3+} phosphors exhibited typical green emission assigned to the 4f–4f transition of Tb^{3+} under excitation at 254 nm. Under near-UV (365 nm) excitation, $Ba_3La_2(BO_3)_4$:Ce^{3+},Tb^{3+} phosphors showed both a blue emission band and green emission peaks due to Ce^{3+} and Tb^{3+}, respectively. By optimizing the composition, cyan-blue emission with high color purity (CIE chromaticity coordinate values $x = 0.2557$ and $y = 0.3839$) was obtained for the $Ba_3La_2(BO_3)_4$:0.05Ce^{3+},0.03Tb^{3+} phosphor, and the internal quantum efficiency of the phosphor at the excitation wavelength of 365 nm is estimated to be 50%. The dental glazing paste prepared by mixing organic binder, $Ba_3La_2(BO_3)_4$:Ce^{3+},Tb^{3+} phosphors, and low T_g glass was successfully vitrified when it was heated at 600 and 700 °C, and showed high chemical stability of the luminescence properties in acidic aqueous solution (pH = 4).

Introduction

Phosphors have been widely applied in displays and lamps and are significantly important materials in our daily life. In particular, rare earth ion doped phosphors have been widely studied for application in a variety of luminescent materials such as general solid state lighting, display devices, electroluminescent devices, optical information storage, X-ray detectors, and TV monitors due to their excellent photoluminescence properties.[1–3] Among these phosphor applications, phosphor-converted light-emitting diodes (pc-LEDs) have great potential in the field of high performance solid-state lighting system such as flashlights, indicating lights, and automobile headlights because of their lower power consumption, long life, high color rending index and conversion efficiency.[4–6]

Recently, many investigations have been devoted to the search for new application fields for phosphor materials, such as plant growth,[7–11] optical sensors,[12–17] cosmetics[18,19] anti-counterfeiting[20] and road signs/lanes.[21,22] In addition, the phosphors have been used in the dental field to enhance the aesthetics of artificial crowns and restoration.[21–29] Under UV-light irradiation, human natural teeth emit cyan blue color with peak at 450 nm and the photoluminescence (PL) properties of teeth make whiter and brighter for human natural teeth in daylight.[30] The artificial crowns and restorative materials can match the shade of the natural teeth to satisfy aesthetic requirements by adding phosphors or pigments.[25,26,31] The studies to develop the paste containing phosphor powder and glass frit, which called the dental glazing, are recently conducted to improve the aesthetics of artificial crowns and restoration.

In the present study, therefore, we have focused on the Ce^{3+} and Tb^{3+} co-doped phosphors to realize a development of the dental glazing paste in accordance with aesthetic requirements for artificial teeth. It is well-known that the Tb^{3+} ion-doped phosphors show the sharp green emission due to the 4f–4f transition of Tb^{3+} under UV excitation and the Ce^{3+} ion-doped phosphors show the broad blue emission due to the 5d–4f transition of Ce^{3+} under UV excitation.[32–37] The PL properties of the Ce^{3+} and Tb^{3+} co-doped phosphors have been investigated

[a]*Electronic Convergence Materials Division, Optic & Electronic Component Materials Center, Korea Institute of Ceramic Engineering and Technology, Jinju 52851, Korea. E-mail: ktwcj@naver.com; skim80@kicet.re.kr*

[b]*Division of Materials Science and Engineering & Convergence Technology, Gyeongsang National University, Jinju 52828, Korea*

[c]*Department of Chemistry, Pusan National Univeristy, Busan 46241, Korea*

[d]*Advanced Resources Team, Yeongwol Industrial Promotion Agency, Gangwon-do 26240, Korea. E-mail: bsbae@yipa.or.kr*

† Electronic supplementary information (ESI) available. See DOI: 10.1039/d1ra04384f

by several researchers.[38–45] Although Tb^{3+} ion-doped phosphors have a weak optical absorption in near-UV region, the Ce^{3+} and Tb^{3+} co-doped phosphors show a strong green emission under excitation which is considered to be due to the energy transfer from Ce^{3+} to Tb^{3+}. These phosphors exhibit a color tunable emission by changing the concentration of Ce^{3+} and Tb^{3+} ions in the host lattice. These results indicate that the Ce^{3+} and Tb^{3+} co-doped phosphors can be expected as one of the suitable candidate for the cyan blue emission phosphor to achieve aesthetic requirements for teeth application.

In this study, using Ce^{3+} and Tb^{3+} ions as activators, cyan blue emitting $Ba_3La_2(BO_3)_4$:Ce^{3+},Tb^{3+} phosphors were synthesized by a conventional solid state reaction and the photoluminescence properties were characterized. The dental glazing pastes were prepared by mixing the as-prepared Tb^{3+}/Ce^{3+} co-doped phosphor powders, an organic binder and a low T_g glass frits with a composition of $(K,Na)_2O$–B_2O_3–Al_2O_3–SiO_2. The photoluminescence properties and chemical stability against acid aqueous solution of the dental glazing pastes were investigated.

Experimental

Ce^{3+}/Tb^{3+} doped $Ba_3La_2(BO_3)_4$ phosphors were synthesized by a conventional solid state reaction method. $BaCO_3$ (Junsei Chemical Co., Ltd., 99%), La_2O_3 (Daejung Chemical & Metal Co., Ltd., 99.9%), B_2O_3 (Junsei, >95%), CeO_2 (LTS, 99.98%), Tb_4O_7 (LTS, 99.95%) were used as starting materials with no further purification. In Ce^{3+}/Tb^{3+} doped $Ba_3La_2(BO_3)_4$ phosphor, the amount of Ce^{3+} was adjusted between 1 to 15 mol% and the Tb^{3+} content was varied from 1 to 15 mol%. These raw materials were mixed in a stoichiometric ratio using an agate mortar for 5 times, and then the mixture was calcined at 800 °C for 6 h in a flow of 5% H_2–95% N_2 gas to reduce Ce^{4+} to Ce^{3+} and Tb^{4+} to Tb^{3+}. After the calcination, the samples were reground in a mortar and heated again at 1200 °C for 6 h in a flow of 5% H_2–95% N_2 gas.

To prepare the dental glazing paste, the as-prepared Tb^{3+}/Ce^{3+} co-doped phosphor powders mixed with an organic binder and a low T_g glass with a composition of $(K,Na)_2O$–B_2O_3–Al_2O_3–SiO_2. Then the homogeneous mixture was mixed and aged using wet ball milling process at room temperature for 24 h. The as-prepared dental glazing pastes coated on alumina plate using brushing method and then heated at 300–700 °C for 0.5 h in air atmosphere.

The crystal structure of the resultant powder samples was identified using X-ray powder diffraction (XRD, Bruker D8 advance), and the detailed crystallographic data were obtained by Rietveld analysis using the RIETAN-FP package.[46] To determine the valence state of Ce and Tb ion in the $Ba_3La_2(BO_3)_4$:Ce^{3+},Tb^{3+} phosphor, X-ray photoelectron spectroscopy (XPS; JEOL, JPS-9000) was measured at room temperature. The morphology of the samples was characterized using scanning electron microscope (JEOL, JSM6700F). The photoluminescence emission (PL) and excitation (PLE) spectra were measured at room temperature using a fluorescence spectrophotometer (PSI, DARSA PRO 3400). PL spectra of Ce^{3+}/Tb^{3+} doped $Ba_3La_2(BO_3)_4$ phosphor were obtained for excitation at 365 nm, and PLE spectra were recorded for emission at 450 and 543 nm. The internal quantum yield was measured using a spectrophotometer (PSI, DARSA PRO 3400) with a fluorescence integrating sphere unit (PSI, DARSA PRO 3400) at excitation wavelength of 365 nm. The photoluminescence properties of dental glazing paste were also characterized using a fluorescence spectrophotometer (PSI, DARSA PRO 3400). The time-resolved photoluminescence (TR-PL) was carried out using a confocal microscope (MicroTime-200, Picoquant, Germany). A single-mode pulsed diode laser (375 nm with 30 ps pulse width and average power of ~1 μW operating in 1 MHz repetition rate) was used as an excitation source. To evaluate the chemical stability of the photoluminescence properties for the dental glazing paste, the acid resistance was investigated with HCl aqueous solution (pH = 4).

Results and discussion

Crystal structure analysis of Ce^{3+}/Tb^{3+} doped $Ba_3La_2(BO_3)_4$ phosphors

Crystallographic data and structure refinement parameters of the Rietveld refinement of the XRD patterns of the Ce^{3+}/Tb^{3+} doped $Ba_3La_2(BO_3)_4$ phosphor are summarized in Table 1, and the representative XRD pattern of the $Ba_3La_2(BO_3)_4$ host material is shown in Fig. 1. The representative XRD patterns of the Ce^{3+}/Tb^{3+} doped $Ba_3La_2(BO_3)_4$ phosphors are shown in Fig. S1–S3† and the refined structural parameters of the $Ba_3La_2(BO_3)_4$ host material and Ce^{3+}/Tb^{3+} doped $Ba_3La_2(BO_3)_4$ phosphors are summarized in Tables S1–S4.† The data of the orthorhombic structure $Ba_3La_2(BO_3)_4$ from the inorganic crystal structure database (ICSD no. 98-003-9277) were used for the starting model. As shown in Table 1, the final *R*-factor

Table 1 Crystallographic data of $Ba_3La_2(BO_3)_4$ and Ce^{3+}/Tb^{3+} doped $Ba_3La_2(BO_3)_4$ phosphors

Formula	$Ba_3La_2(BO_3)_4$	$Ba_3(La,Ce)_2(BO_3)_4$	$Ba_3(La,Tb)_2(BO_3)_4$	$Ba_3(La,Ce,Tb)_2(BO_3)_4$
Crystal system	Orthorhombic	Orthorhombic	Orthorhombic	Orthorhombic
Space group	*Pnma*	*Pnma*	*Pnma*	*Pnma*
a (nm)	0.77735(4)	0.77692(5)	0.77708(2)	0.77610(2)
b (nm)	1.70989(1)	1.71059(12)	1.70686(5)	1.70481(4)
c (nm)	0.90422(3)	0.90271(4)	0.90220(2)	0.90225(1)
R_{wp} (%)	10.99	11.36	10.00	10.64
R_p (%)	8.10	8.40	7.31	7.84
S (%)	2.36	2.65	2.57	3.08

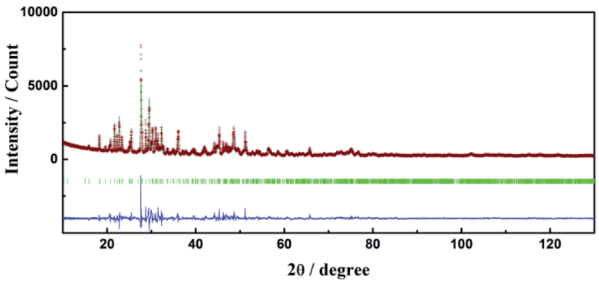

Fig. 1 Rietveld refinement result for X-ray powder diffraction data of $Ba_3La_2(BO_3)_4$. Red symbol: measured pattern, green solid line: calculated pattern, blue solid line: difference between their intensities.

values, R_{wp}, R_p, and S, converged to 10.99, 8.10, and 2.36, respectively, which verify the phase purity of the as-prepared sample. The representative XRD pattern of $Ba_3La_2(BO_3)_4$ was well indexed to the reported data and no impurity phases were detected in the XRD pattern. The final refined results confirm a single phase of the $Ba_3La_2(BO_3)_4$ that is crystallized in a orthorhombic structure in space group *Pnma* (no. 62) with refined lattice parameters $a = 0.77735(4)$ nm, $b = 1.70989(1)$ nm, $c = 0.90422(3)$ nm, and $V = 1.20187$ nm^3. A schematic of the $Ba_3La_2(BO_3)_4$ crystal structure is shown in Fig. 2, produced using VESTA.[47] According to the crystal structure analysis, Ba^{2+} and La^{3+} ions occupied in three different dodecahedral sites (8d and 4c) and there are three kinds of boron sites (8d and 4c) with 3-fold coordination. The lattice volume of the $Ba_3La_2(BO_3)_4$ phase decreased with doping the Ce^{3+} and Tb^{3+} in the crystal lattice, which indicates that the small size of Ce^{3+} (ionic radius: 0.1143 nm for 8 coordination[48]) and Tb^{3+} (ionic radius: 0.1040 nm for 8 coordination[48]) are successfully substituted into the larger La^{3+} ions sites (ionic radius: 0.1160 nm for 8 coordination[48]). Fig. 3 shows the XRD patterns of $Ba_3La_2(BO_3)_4$:Ce^{3+}, $Ba_3La_2(BO_3)_4$:Tb^{3+}, $Ba_3La_2(BO_3)_4$:Ce^{3+},Tb^{3+} phosphor samples with different concentrations. The XRD patterns of all samples were in good agreement with a single phase of highly crystalline orthorhombic structure (ICSD no. 98-003-9277) with space group *Pnma* (#62). With increasing the Ce^{3+} and Tb^{3+} ion contents in the Ce^{3+}/Tb^{3+} doped $Ba_3La_2(BO_3)_4$ phosphors, a peak shift to a higher diffraction angle is observed because La^{3+} in the host

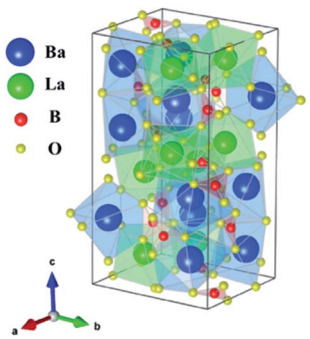

Fig. 2 A schematic of the $Ba_3La_2(BO_3)_4$ crystal structure.

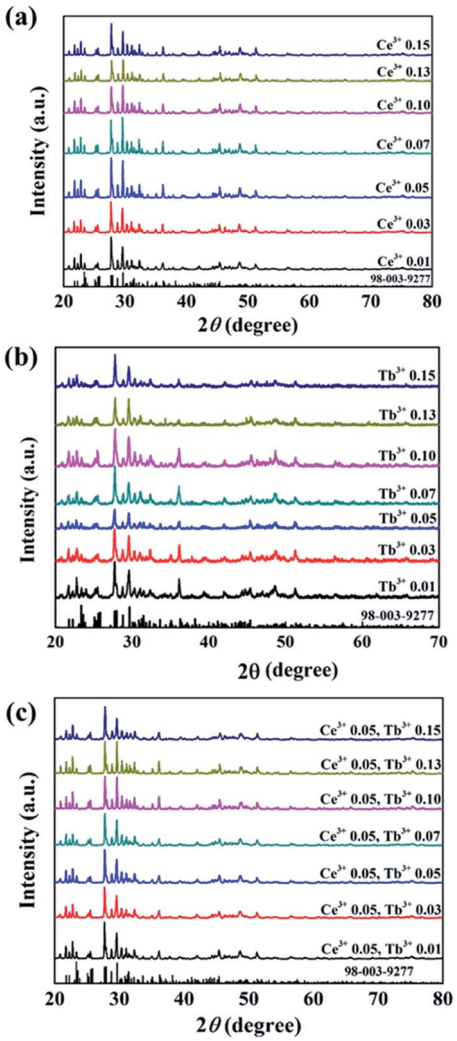

Fig. 3 XRD patterns of (a) $Ba_3La_2(BO_3)_4$:Ce^{3+}, (b) $Ba_3La_2(BO_3)_4$: Tb^{3+}, (c) $Ba_3La_2(BO_3)_4$:Ce^{3+},Tb^{3+} phosphors doped with different concentrations and $Ba_3La_2(BO_3)_4$ reference (ICSD 98-003-9277).

material is partially substituted with the smaller Ce^{3+} and Tb^{3+} ions to form solid solutions. To investigate the valence state of Ce and Tb ions, binding energy of electrons in $Ba_3La_2(BO_3)_4$:Ce^{3+},Tb^{3+} phosphors was measured using XPS and the result is shown in Fig. S4.† The Ce 3d and Tb 3d XPS spectra are well known to split into two peaks of $3d_{3/2}$ and $3d_{5/2}$ due to the spin–orbital interaction. The XPS spectra of both Ce 3d and Tb 3d state exhibit two clear peaks at 889.9 eV ($3d_{3/2}$) and 901.9 eV ($3d_{5/2}$), and at 1242.8 eV ($3d_{3/2}$) and 1275.9 eV ($3d_{5/2}$), respectively, which can be assigned to those of 3+ oxidation state of Ce and Tb ions. In addition, no peaks that would suggest the presence of other oxidation states of Ce and Tb ions were observed. These results support that the Ce and Tb ions successfully substituted in the La^{3+} sites as Ce^{3+} and Tb^{3+} in the $Ba_3La_2(BO_3)_4$ host lattice. The morphologies of the Ce^{3+}/Tb^{3+} doped $Ba_3La_2(BO_3)_4$ phosphors were observed by SEM as seen in Fig. 4. The particles of all powder samples were composed of angular-shape fine grain with the average size of around 5–10 μm.

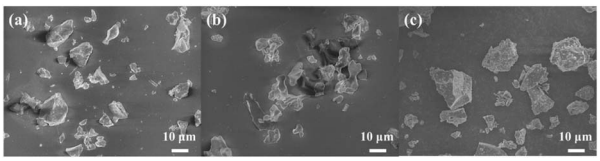

Fig. 4 SEM images of (a) $Ba_3La_2(BO_3)_4$:Ce^{3+}, (b) $Ba_3La_2(BO_3)_4$: Tb^{3+}, (c) $Ba_3La_2(BO_3)_4$:Ce^{3+},Tb^{3+} phosphors.

Photoluminescence properties of Ce^{3+} doped $Ba_3La_2(BO_3)_4$ phosphor

The photoluminescence emission (PL) and excitation (PLE) spectra of $Ba_3La_2(BO_3)_4$:Ce^{3+} phosphors with different concentration of Ce^{3+} ions are presented in Fig. 5. The PLE spectra recorded by monitoring the emission at 470 nm exhibited a broad excitation band from 270 to 400 nm, which was attributed to 4f → 5d transition of Ce^{3+} ions. The PL spectra of $Ba_3La_2(BO_3)_4$:Ce^{3+} phosphors recorded under 365 nm excitation showed a broad non-symmetry blue emission band from 400 nm to 650 nm with a maximum peak at 470 nm due to 5d → 4f transition of Ce^{3+} ions. The emission of Ce^{3+} usually includes two bands of the transitions of 5d-excited state to $^2F_{7/2}$ and $^2F_{5/2}$ states, and the emission spectra seem to consist of two of them in a single band. The emission peak wavelength of the Ce^{3+} 5d → 4f transition shifts to the longer wavelength (lower energy) direction with increasing Ce^{3+} concentration for the sample, which can be attributed to the change of the crystal field strength around Ce^{3+} in the host lattice. The crystal field strength increases with increasing the amount of Ce^{3+} substitution for La^{3+} in the $Ba_3La_2(BO_3)_4$ lattice because the average bond length of Ce^{3+}–O^{2-} becomes progressively shorter by lattice shrinkage.[49] The emission peak intensity of $Ba_3La_2(BO_3)_4$:Ce^{3+} phosphors was increased with the Ce^{3+} concentration up to 0.05 mol%, and then decreased probably due to the concentration quenching effect. The internal quantum yield of the 0.05 mol% Ce^{3+} doped $Ba_3La_2(BO_3)_4$ phosphor at the excitation wavelength of 365 nm was estimated to be 50%. Thus, the optimum concentration of Ce^{3+} ions was confirmed to be 0.05, and it was kept as a constant value to prepare Ce^{3+}/Tb^{3+} co-doped $Ba_3La_2(BO_3)_4$ phosphors.

Photoluminescence properties of Tb^{3+} doped $Ba_3La_2(BO_3)_4$ phosphor

Fig. 6 shows the PL and PLE spectra of $Ba_3La_2(BO_3)_4$:Tb^{3+} phosphors with different concentration of Tb^{3+} ions. The PLE spectra recorded by monitoring the emission at 543 nm, there are a broad band from 225 to 300 nm, corresponding to the spin-allowed energy transition from the $4f^8$ to $4f^7$5d configuration of Tb^{3+}. A number of small absorption peaks at 300–400 nm correspond to the spin-forbidden 4f–4f transition ($^7F_6$ → $^5L_{1,5,10}$, $^7F_6$ → $^5D_3$). Under 254 nm excitation, the $Ba_3La_2(BO_3)_4$:Tb^{3+} phosphors exhibited a well-known characteristic Tb^{3+} green emission, and no self-activated emission was observed in the undoped samples. The emission peaks of

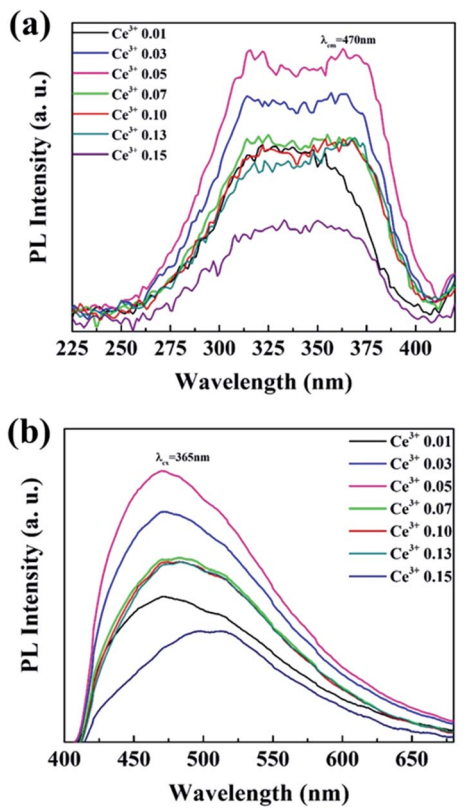

Fig. 5 The (a) excitation (λ_{em} = 470 nm) and (b) emission (λ_{ex} = 365 nm) and spectra of $Ba_3La_2(BO_3)_4$:Ce^{3+} phosphors with different concentrations of Ce^{3+}.

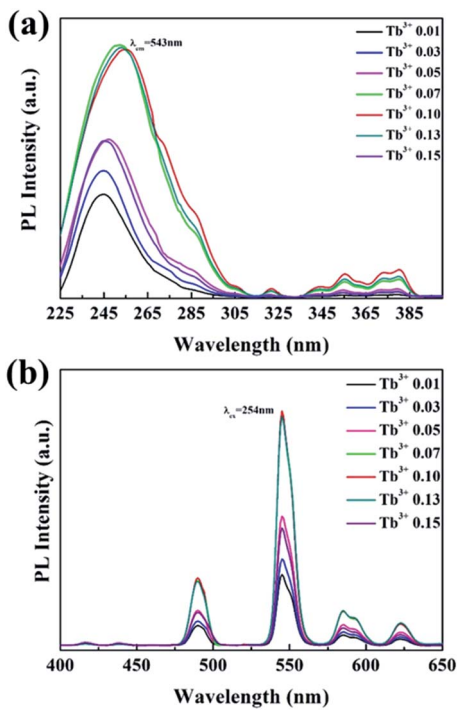

Fig. 6 The (a) excitation (λ_{em} = 543 nm) and (b) emission (λ_{ex} = 254 nm) spectra of $Ba_3La_2(BO_3)_4$ phosphors doped with different concentrations of Tb^{3+}.

$Ba_3La_2(BO_3)_4$:Tb^{3+} phosphors at 490, 547, 585, and 623 nm correspond to the $^5D_4 \rightarrow {}^7F_6$, $^5D_4 \rightarrow {}^7F_5$, $^5D_4 \rightarrow {}^7F_4$, and $^5D_4 \rightarrow {}^7F_3$ transitions of Tb^{3+} ions, respectively.[50–52] The emission intensity of $Ba_3La_2(BO_3)_4$:Tb^{3+} phosphors was increased with increasing the Tb^{3+} concentration up to 0.10, and then decreased due to the concentration quenching effect. In particular, the emission intensity of 0.15 showed a dramatically decrease. The concentration quenching of luminescence is generally observed in phosphor materials in which a large amount of luminescence ion is doped into the host lattice.[53,54] By increasing the luminescence ion concentration in host lattice, the distance between two adjacent luminescence ions is decreased and the interaction between the luminescence ions is enhanced, which usually results in the concentration quenching due to the nonradiative energy transfer between two luminescence ions.[53,54] The internal quantum yield of the 0.10 mol% Tb^{3+} doped $Ba_3La_2(BO_3)_4$ phosphor at the excitation wavelength of 365 nm was estimated to be 60%.

Photoluminescence properties of Ce^{3+} and Tb^{3+} doped $Ba_3La_2(BO_3)_4$ phosphor

To develop the cyan blue-emitting phosphors with similar to that of human teeth, Ce^{3+} and Tb^{3+} co-activated $Ba_3La_2(BO_3)_4$ phosphors synthesized and their optical properties were characterized. In Ce^{3+}/Tb^{3+} co-activated $Ba_3La_2(BO_3)_4$ phosphors, the concentration of Ce^{3+} was fixed at the optimal value of 0.05 mol% and the concentration of Tb^{3+} was varied in the range of 0.01–0.15 mol%. The PLE and PL spectra of Ce^{3+}/Tb^{3+} co-activated $Ba_3La_2(BO_3)_4$ phosphors are shown in Fig. 7. The PLE spectra monitored at 547 nm (Tb^{3+} $^5D_4$–$^7F_5$ transition emission) consists of two strong broad bands with peaks at about 247 nm and 330 nm due to the $4f^8 \rightarrow 4f^7$5d transition of Tb^{3+} and $4f^1 \rightarrow 4f^0$5d transition of Ce^{3+}, respectively. These PLE spectra are evidence of energy transfer from Ce^{3+} to Tb^{3+} in $Ba_3La_2(BO_3)_4$:Ce^{3+},Tb^{3+} phosphors. The intensities of the optical absorption bands due to $4f^8 \rightarrow 4f^7$5d transition of Tb^{3+} and $4f^1 \rightarrow 4f^0$5d transition of Ce^{3+} were effectively enhanced by increasing the Tb^{3+} ion contents in $Ba_3La_2(BO_3)_4$:Ce^{3+},Tb^{3+} phosphors. Under the excitation of 365 nm, the emission spectra exhibit a broad band of Ce^{3+} ions in the blue light region and a series of strong emission lines at 490, 545, 585, and 623 nm due to the $^5D_4$–^7F_J ($J = 6$, 5, 4, and 3) transitions of Tb^{3+} ions in which the green emission line at 542 nm from $^5D_4$–$^7F_5$ transitions dominate. Although the emission spectra of the phosphors were recorded for excitation at 365 nm (optical absorption due to Ce^{3+}), the Ce^{3+} emission intensity increased with increasing the concentration of Tb^{3+} in $Ba_3La_2(BO_3)_4$:Ce^{3+},Tb^{3+} phosphors, whereas Tb^{3+} emission effectively enhanced. The energy-transfer efficiency of $Ce^{3+} \rightarrow Tb^{3+}$ in $Ba_3La_2(BO_3)_4$:Ce^{3+},Tb^{3+} phosphors increased remarkably with increasing the Tb^{3+} contents. These results are evidence of energy transfer from Ce^{3+} to Tb^{3+} in the $Ba_3La_2(BO_3)_4$:Ce^{3+},Tb^{3+} phosphors. As shown in Fig. 7 inset, it can be found that color-tunable blue-to-green emission can be obtained with increasing Tb^{3+} content due to $Ce^{3+} \rightarrow Tb^{3+}$ energy transfer. Additionally, the CIE coordinates for the $Ba_3La_2(BO_3)_4$:Ce^{3+},Tb^{3+} phosphors

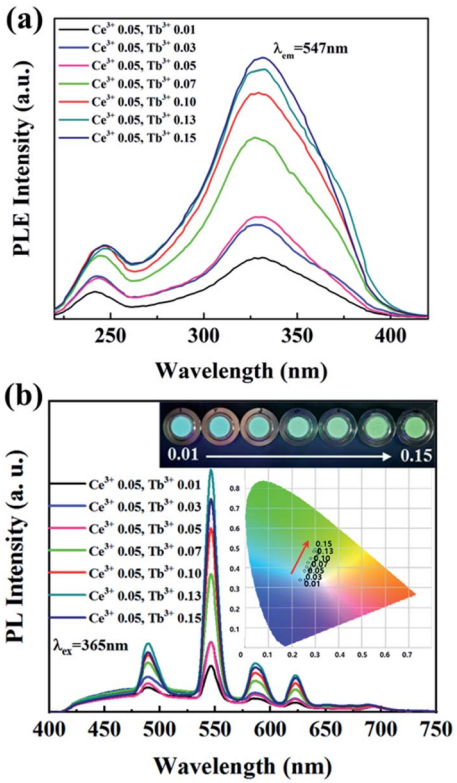

Fig. 7 The (a) excitation (λ_{em} = 547 nm) and (b) emission (λ_{ex} = 365 nm) spectra of $Ba_3La_2(BO_3)_4$:Ce^{3+},Tb^{3+} phosphors with different concentrations of Tb^{3+}.

could be changed from the ($x = 0.2368$, $y = 0.3388$; blue) to ($x = 0.3006$, $y = 0.4914$; green) by controlling the different emission compositions of the Ce^{3+} and Tb^{3+} contents. Among the different amount of Ce^{3+}/Tb^{3+} co-doped $Ba_3La_2(BO_3)_4$ phosphors, the emission color of the $Ba_3La_2(BO_3)_4$:0.05Ce^{3+},0.03Tb^{3+} phosphor is very close to cyan light of commercial materials for use in dental glassing.

To determine the energy transfer from Ce^{3+} to Tb^{3+} in $Ba_3La_2(BO_3)_4$:Ce^{3+},Tb^{3+} phosphors, the luminescence lifetime of the phosphors were recorded by confocal microscope. Fig. 8 illustrates the decay curves of $Ba_3La_2(BO_3)_4$:0.05Ce^{3+} and $Ba_3La_2(BO_3)_4$:0.05Ce^{3+},0.13Tb^{3+} phosphors monitored at 470 nm for Ce^{3+} emission. The decline of lifetime further demonstrated the presence of energy transfer from Ce^{3+} to Tb^{3+}. Additionally, efficiency of energy transfer (η_{ET}) between Ce^{3+} and Tb^{3+} can be calculated by following equation:[55]

$$\eta_{ET} = 1 - \tau/\tau_0$$

where τ and τ_0 represent fluorescence lifetime of phosphors with and without Tb^{3+} doping. The average lifetime of $Ba_3La_2(BO_3)_4$:0.05Ce^{3+},0.13Tb^{3+} phosphors with and without Tb^{3+} doping can be calculated as 14 ns and 11 ns, respectively. It obviously shows that the average lifetime of Ce^{3+} ions decreases with Tb^{3+} ions doping. The efficiency of energy transfer from Ce^{3+} to Tb^{3+} in the $Ba_3La_2(BO_3)_4$:0.05Ce^{3+},0.13Tb^{3+} phosphors was estimated to be approximately 21.5%.

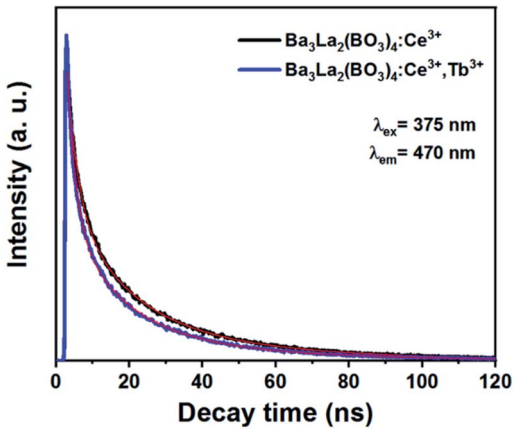

Fig. 8 The decay curves of $Ba_3La_2(BO_3)_4$:0.05Ce^{3+} and $Ba_3La_2(BO_3)_4$:0.05Ce^{3+},0.13Tb^{3+} phosphors.

Characterization of dental glazing paste using Ce^{3+}/Tb^{3+} co-doped $Ba_3La_2(BO_3)_4$ phosphor

The dental glazing paste using the Ce^{3+}/Tb^{3+} co-doped $Ba_3La_2(BO_3)_4$ phosphor was prepared by mixing with an organic binder and a low T_g glass with a composition of $(K,Na)_2O$–B_2O_3–Al_2O_3–SiO_2. The as-prepared dental glazing pastes coated on alumina plate using brushing method and then heated at 300–700 °C for 0.5 h in air atmosphere. Fig. 9 shows the photograph of dental glazing pastes coated on alumina plate and the PL spectra of the dental glazing pastes heated at 300–700 °C for 0.5 h. The pastes heated at 300–500 °C was observed no vitrification, whereas, in the case of the pastes heated at 600 and 700 °C, vitrification was successfully observed. The emission peak intensity of the dental glazing pastes decreases with increasing the heating temperature (Fig. 9(a)). The reduction of the emission intensity of the Ce^{3+} or Eu^{2+} doped phosphors owing to re-heating is well known in phosphor-in-glass (PiG) application.[56–62] The reduction of the emission intensity is well known to be due to the oxidation of Ce^{3+} into Ce^{4+} (or Eu^{2+} into Eu^{3+}) in the phosphors, and the oxidation of luminescence ions usually results in the thermal degradation of the photoluminescence efficiency of the phosphors.[63,64]

To evaluate the chemical stability of the photoluminescence efficiency of the as-prepared dental glazing pastes using the Ce^{3+}/Tb^{3+} co-doped $Ba_3La_2(BO_3)_4$ phosphor, the acid resistance of the as-prepared dental glazing pastes was carried out in HCl aqueous solution (pH = 4). The pH values of drink such as an orange juice, coke, ade and *etc.* is about 3–4. The dental glazing pastes coated on alumina plate, which prepared by heating at 600 °C, was treated with HCl aqueous solution and soaked for 48 h, and then washed with water and dried at 80 °C for 24 h. After the HCl aqueous solution treatment for 48 h, which is very hard condition, the emission intensity of the dental glazing paste was decreased to 85% of the non-treatment sample as shown in Fig. 9(b). This result evidences that the dental glazing paste possesses high resistance to the acid solution.

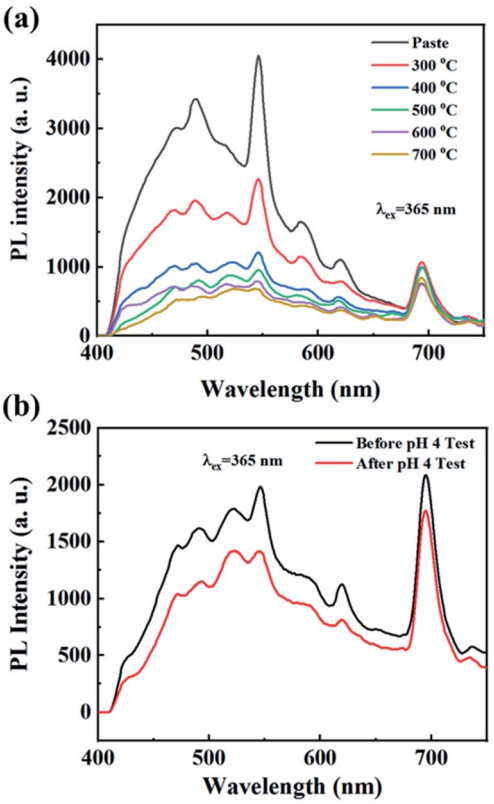

Fig. 9 (a) The photograph of dental glazing pastes coated on alumina plate and the PL spectra of the dental glazing pastes heated at 300–700 °C for 0.5 h, (b) the emission spectra of the dental glazing paste before and after pH 4 test.

Conclusions

In this study, we demonstrated the possibility of the $Ba_3La_2(BO_3)_4$:Ce^{3+},Tb^{3+} phosphors for use in dental glazing paste. The $Ba_3La_2(BO_3)_4$:Ce^{3+},Tb^{3+} phosphors were synthesized in a single phase form by a conventional solid state reaction method. The $Ba_3La_2(BO_3)_4$:Ce^{3+} phosphors showed a asymmetric broad blue emission with maximum peak at 470 nm under excitation at 365 nm due to the 5d → 4f transition of Ce^{3+}, and the maximum emission peak intensity was obtained for the $Ba_3La_2(BO_3)_4$:0.05Ce^{3+}. The $Ba_3La_2(BO_3)_4$:Tb^{3+} phosphors exhibited typical green emission assigned to the 4f–4f transition of Tb^{3+} under excitation at 254 nm, and the highest green emission intensity was obtained for the $Ba_3La_2(BO_3)_4$:0.10Tb^{3+}. Under near-UV (365 nm) excitation, $Ba_3La_2(BO_3)_4$:Ce^{3+},Tb^{3+} phosphors showed both blue emission band and green emission peaks due to the Ce^{3+} and Tb^{3+}, respectively, and the emission color of the phosphors can be tuned from blue to green by changing Ce^{3+}/Tb^{3+} ratio. By optimization of the composition, cyan-blue emission with high color purity was obtained for the $Ba_3La_2(BO_3)_4$:0.05Ce^{3+},0.03Tb^{3+} phosphor, and the CIE chromaticity coordinate values for the phosphor were $x = 0.2557$ and $y = 0.3839$ under excitation at 365 nm, which is close to the cyan-blue emission for natural teeth. The internal quantum efficiency of the phosphor at the excitation wavelength of 365 nm is

estimated to be 50%. To prepare the dental glazing paste, the Ce^{3+}/Tb^{3+} co-doped $Ba_3La_2(BO_3)_4$ phosphor powders mixed with an organic binder and a low Tg glass with a composition of $(K,Na)_2O–B_2O_3–Al_2O_3–SiO_2$. For the samples heated at 600 and 700 °C, the dental glazing paste showed clear vitrification and they showed a high chemical stability of the luminescence properties for acid aqueous solution (pH = 4). These results indicate that the Ce^{3+}/Tb^{3+} co-doped $Ba_3La_2(BO_3)_4$ phosphor are a suitable candidate as a luminescent material to produce the dental glazing paste with a high aesthetic.

Conflicts of interest

There are no conflicts to declare.

Acknowledgements

This work was supported by the Technology Development Program (S2800580) funded by the Ministry of SMEs and Startups (MSS, Korea).

Notes and references

1 N. Avci, J. Musschoot, P. Smet, K. Korthout, A. Avci, C. Detavernier and D. Poelman, Microencapsulation of moisture-sensitive CaS: Eu^{2+} particles with aluminum oxide, *J. Electrochem. Soc.*, 2009, **156**, J333.

2 V. Gapontsev, S. Matitsin, A. Isineev and V. Kravchenko, Erbium glass lasers and their applications, *Opt. Laser Technol.*, 1982, **14**, 189.

3 K. Hirao, S. Todoroki, D. Cho and N. Soga, Room-temperature persistent hole burning of Sm^{2+} in oxide glasses, *Opt. Lett.*, 1993, **18**, 1586.

4 S. Ye, F. Xiao, Y. Pan, Y. Ma and Q. Zhang, Phosphors in phosphor-converted white light-emitting diodes: Recent advances in materials, techniques and properties, *Mater. Sci. Eng., R*, 2010, **71**, 1.

5 S. Pimputkar, J. S. Speck, S. P. DenBaars and S. Nakamura, Prospects for LED lighting, *Nat. Photonics*, 2009, **3**, 180.

6 Y. H. Kim, N. S. Viswanath, S. Unithrattil, H. J. Kim and W. B. Im, phosphor plates for high-power LED applications: challenges and opportunities toward perfect lighting, *ECS J. Solid State Sci. Technol.*, 2017, **7**, R3134.

7 Z. Zhou, M. Xia, Y. Zhong, S. Gai, S. Huang, Y. Tian, X. Lu and N. Zhou, Dy^{3+}@Mn^{4+} co-doped $Ca_{14}Ga_{10-m}Al_mZn_6O^{35}$ far-red emitting phosphors with high brightness and improved luminescence and energy transfer properties for plant growth LED lights, *J. Mater. Chem. C*, 2017, **5**, 8201.

8 Y. Zheng, H. Zhang, Z. Xia, Y. Liu, M. Molokeev and B. Lei, Co-substitution of Y^{3+}/Mg^{2+} for Ca^{2+}/Al^{3+} in $CaAl_{12}O_{19}$:Mn^{4+} phosphors: local structure evolution, photoluminescence tuning and application for plant growth LEDs, *J. Mater. Chem. C*, 2018, **6**, 4217.

9 X. Yang, Y. Zhang, X. Zhang, J. Chen, H. Huang, D. Wang, X. Chai, G. Xie, M. S. Molokeev and H. Zhang, Facile synthesis of the desired red phosphor $Li_2Ca_2Mg_2Si_2N_6$:Eu^{2+} for high CRI white LEDs and plant growth LED device, *J. Am. Ceram. Soc.*, 2020, **103**, 1773.

10 M. Rajendran and S. Vaidyanathan, Zero-concentration quenching: a novel Eu^{3+} based red phosphor with non-layered crystal structure for white LEDs and NaSrY $(MoO_4)_3$:Sm^{3+} based deep-red LEDs for plant growth, *Dalton Trans.*, 2020, **49**, 9239.

11 S. Gu, M. Xia, C. Zhou, Z. Kong, M. S. Molokeev, L. Liu, W.-Y. Wong and Z. Zhou, Red shift properties, crystal field theory and nephelauxetic effect on Mn^{4+}-doped $SrMgAl_{10-y}Ga_yO_{17}$ red phosphor for plant growth LED light, *Chem. Eng. J.*, 2020, **396**, 125208.

12 B. Yan, Y. Wei, W. Wang, M. Fu and G. Li, Red-tunable LuAG garnet phosphors *via* $Eu^{3+}\rightarrow Mn^{4+}$ energy transfer for optical thermometry sensor application, *Inorg. Chem. Front.*, 2021, **8**, 746.

13 Y. Hu, F. Zhou, X. Tian, C. Ji, Z. Huang, J. Wen, F. Luo, Z. Chen, X. Liu and Y. Peng, $CaSnO_3$: Pr^{3+} phosphor for new application in temperature sensing, *Spectrochim. Acta, Part A*, 2020, **243**, 118799.

14 G. Xiang, X. Liu, Q. Xia, S. Jiang, X. Zhou, L. Li, Y. Jin, L. Ma, X. Wang and J. Zhang, Deep-Tissue Temperature Sensing Realized in BaY_2O_4:Yb^{3+}/Er^{3+} with Ultrahigh Sensitivity and Extremely Intense Red Upconversion Luminescence, *Inorg. Chem.*, 2020, **59**, 11054.

15 G. Xiang, Q. Xia, X. Liu, Y. Wang, S. Jiang, L. Li, X. Zhou, L. Ma, X. Wang and J. Zhang, Upconversion nanoparticles modified by Cu_2S for photothermal therapy along with real-time optical thermometry, *Nanoscale*, 2021, **13**, 7161.

16 H. Suo, X. Zhao, Z. Zhang, Y. Wu and C. Guo, Upconverting $LuVO_4$:$Nd^{3+}/Yb^{3+}/Er^{3+}$@SiO_2@Cu_2S Hollow Nanoplatforms for Self-monitored Photothermal Ablation, *ACS Appl. Mater. Interfaces*, 2018, **10**, 39912.

17 H. Suo, X. Zhao, Z. Zhang and C. Guo, Ultra-sensitive optical nano-thermometer $LaPO_4$:Yb^{3+}/Nd^{3+} based on thermo-enhanced NIR-to-NIR emissions, *Chem. Eng. J.*, 2020, **389**, 124506.

18 A. Verma and A. Verma, Synthesis, characterization, mechano-luminescence, thermoluminescence, and antibacterial properties of $SrMgAl_{10}O_{17}$: Eu phosphor, *J. Alloys Compd.*, 2019, **802**, 394.

19 S. W. Kim, T. Hasegawa, M. Watanabe, K. Sugimoto, Y. Saito, K. Uematsu, K. Toda and M. Sato, Environmentally friendly $Rb_3V_5O_{14}$ fluorescent red pigment, *Dyes Pigm.*, 2017, **136**, 219.

20 D. Jiang and C. N. Chong, *2nd International Conference on Anti-counterfeiting, Security and Identification, China*, August, 2008.

21 B. Zhu, C. Song, Z. Guo, Y. Zhang and Z. Zhou, Effectiveness of Active Luminous Lane Markings on Highway at Night: A Driving Simulation Study, *Sustainability*, 2021, **13**, 1043.

22 J. I. Park, S. H. Jeong and I. W. Cheong, Microencapsulation of $SrAl_2O_4$:Eu^{2+}, Dy^{3+} Phosphorescent Phosphor for Enhanced Visibility of Road Lanes, *J. Adhes. Interface*, 2016, **17**, 110.

23 I. Ahmad, Anterior dental aesthetics: Dental perspective, *Br. Dent. J.*, 2005, **199**, 135.

24 W. Buchalla, Comparative fluorescence spectroscopy shows differences in noncavitated enamel lesions, *Caries Res.*, 2005, **39**, 150.

25 P.-H. Chuang, Y.-J. Lai, C. C. Lin, T.-M. Wang, H. Yang, L.-D. Lin and R.-S. Liu, Facile dental resin composites with tunable fluorescence by tailoring Cd-free quantum dots, *RSC Adv.*, 2013, **3**, 16639.

26 Y. K. Lee, Fluorescence properties of human teeth and dental calculus for clinical applications, *J. Biomed. Opt.*, 2015, **20**, 040901.

27 A. A.-R. S. Marouf and Y. A. Khairallah, Photoemission Spectra of Sound Tooth and Those of Different Carious Stages, *Eur. Biophys. J.*, 2019, **7**, 23.

28 D. Goloshchapov, P. Seredin, D. Minakov and E. Domashevskaya, Photoluminescence Properties of Nanoporous Nanocrystalline Carbonate-Substituted Hydroxyapatite, *Opt. Spectrosc.*, 2018, **124**, 187.

29 X. Li, C. Luo, Q. Fu, C. Zhou, M. Ruelas, Y. Wang, J. He, Y. Wang, Y. S. Zhang and J. Zhou, A Transparent, Wearable Fluorescent Mouthguard for High-Sensitive Visualization and Accurate Localization of Hidden Dental Lesion Sites, *Adv. Mater.*, 2020, **32**, 2000060.

30 H. Panzeri, L. T. Fernandes and C. J. Minelll, Spectral fluorescence of direct anterior restorative materials, *Aust. Dent. J.*, 1977, **22**, 458.

31 A. S. Hermanson, M. A. Bush, R. G. Miller and P. J. Bush, Ultraviolet illumination as an adjunctive aid in dental inspection, *J. Forensic Sci.*, 2008, **53**, 408.

32 Z. Sun, Z. Zhu, Z. Guo, Z.-c. Wu, Z. Yang, T. Zhang and X. Zhang, Electronic structure and luminescent properties of Ce^{3+}-doped $Ba_3Lu_2B_6O_{15}$, a high-efficient blue-emitting phosphor, *Ceram. Int.*, 2019, **45**, 7143.

33 S. W. Kim, T. Masui, H. Matsushita and N. Imanaka, Enhancement in photoluminescence of $Gd_2O_2CO_3$:Tb^{3+} submicron particles by introducing yttrium into the oxycarbonate lattice, *J. Electrochem. Soc.*, 2010, **157**, J181.

34 K. Park, D. Hakeem, J. Pi and S. Kim, Improvement of photoluminescence properties of Ce^{3+}-doped $CaSrAl_2SiO_7$ phosphors by charge compensation with Li^+ and Na^+, *Ceram. Int.*, 2018, **44**, 1929.

35 R. Yu, J. Wang, M. Zhang, J. Zhang, H. Yuan and Q. Su, A new blue-emitting phosphor of Ce^{3+}-activated $CaLaGa_3S_6O$ for white-light-emitting diodes, *Chem. Phys. Lett.*, 2008, **453**, 197.

36 S. W. Kim, K. Jyoko, T. Masui and N. Imanaka, Synthesis of green-emitting (La,Gd)OBr: Tb^{3+} phosphors, *Materials*, 2010, **3**, 2506.

37 S. Zhang, Z. Mu, Y. Lv, L. Fan, Y. Li, G. Ju and Y. Hu, White-light long persistent luminescence of Tb^{3+}-doped $Y_3Al_2Ga_3O_{12}$ phosphor, *J. Alloys Compd.*, 2017, **729**, 418.

38 Y. Li, W. Chen, L. Zhao, D. Meng, Y. Zhang and C. Wang, Ce^{3+} and Tb^{3+} activated $Ba_3P_4O_{13}$ phosphors based on energy transfer behavior, *New J. Chem.*, 2017, **41**, 14876.

39 M. Jose and A. Lakshmanan, Ce^{3+} to Tb^{3+} energy transfer in alkaline earth (Ba, Sr or Ca) sulphate phosphors, *Opt. Mater.*, 2004, **24**, 651.

40 P. Liang, Co-existence phenomenon of Ce^{3+}/Ce^{4+} and Tb^{3+} in Ce/Tb co-doped $Zn_2(BO_3)(OH)_{0.75}F_{0.25}$ phosphor: luminescence and energy transfer, *Adv. Powder Technol.*, 2019, **30**, 974.

41 S. Sun, L. Wu, H. Yi, L. Wu, J. Ji, C. Zhang, Y. Zhang, Y. Kong and J. Xu, Energy transfer between Ce^{3+} and Tb^{3+} and the enhanced luminescence of a green phosphor SrB_2O_4:Ce^{3+},Tb^{3+}, Na^+, *Opt. Mater. Express*, 2016, **6**, 1172.

42 Y. Li, X. Wei, M. Yin and Y. Tao, Energy transfer processes in Ce^{3+} and Tb^{3+} co-doped $Ln_2Si_2O_7$ (Ln = Y, Gd), *Opt. Mater.*, 2011, **33**, 1239.

43 D. Jia, J. Zhu and B. Wu, Luminescence and energy transfer in $CaAl_4O_7$: Tb^{3+}, Ce^{3+}, *J. Lumin.*, 2001, **93**, 107.

44 S. Lee and S. Park, Preparation and luminescent properties of Tb^{3+} and Tb^{3+}–Ce^{3+} doped $Ba_9Y_2Si_6O_{24}$ phosphors, *J. Lumin.*, 2013, **143**, 215.

45 Z. Xia and R.-S. Liu, Tunable blue-green color emission and energy transfer of $Ca_2Al_3O_6F$:Ce^{3+},Tb^{3+} phosphors for near-UV white LEDs, *J. Phys. Chem. C*, 2012, **116**, 15604.

46 F. Izumi and K. Momma, Three-Dimensional Visualization in Powder Diffraction, *Solid State Phenom.*, 2007, **130**, 15.

47 K. Momma and F. Izumi, VESTA: a three-dimensional visualization system for electronic and structural analysis, *J. Appl. Crystallogr.*, 2008, **41**, 653.

48 R. D. Shannon, Revised effective ionic radii and systematic studies of interatomic distances in halides and chalcogenides, *Acta Crystallogr., Sect. A: Cryst. Phys., Diffr., Theor. Gen. Crystallogr.*, 1976, **32**, 751.

49 M. A. Lim, J. K. Park, C. H. Kim, H. D. Park and M. W. Han, Luminescence characteristics of green light emitting Ba_2SiO_4:Eu^{2+} phosphor, *J. Mater. Sci. Lett.*, 2003, **22**, 1351.

50 D. Hakeem, J. Pi, S. Kim and K. Park, New $Y_2LuCaAl_2SiO_{12}$:Ln (Ln= Ce^{3+}, Eu^{3+}, and Tb^{3+}) phosphors for white LED applications, *Inorg. Chem. Front.*, 2018, **5**, 1336.

51 D. Hakeem, J. Pi, G. Jung, S. Kim and K. Park, Structural and photoluminescence properties of $La_{1-x}NaCaGa_3PZrO_{12}$ doped with Ce^{3+}, Eu^{3+}, and Tb^{3+}, *Dyes Pigm.*, 2019, **160**, 234.

52 D. Hakeem, D. Kim, S. Kim and K. Park, Crystal structure and photoluminescence properties of novel garnet $Y_{2-x}LaCaGa_3ZrO_{12}$:xLn^{3+} (Ln = Eu and Tb) phosphors, *Dyes Pigm.*, 2019, **163**, 715.

53 T. Honma, K. Toda, Z.-G. Ye and M. Sato, Concentration quenching of the Eu^{3+}-activated luminescence in some layered perovskites with two-dimensional arrangement, *J. Phys. Chem. Solids*, 1998, **59**, 1187.

54 J. Hölsä, M. Leskelä and L. Niinistö, Concentration quenching of Tb^{3+} luminescence in LaOBr and Gd_2O_2S phosphors, *Mater. Res. Bull.*, 1979, **14**, 1403.

55 U. Caldiño, A. Speghini, E. Álvarez, S. Berneschi, M. Bettinelli, M. Brenci and G. C. Righini, Spectroscopic characterization and optical waveguide fabrication in Ce^{3+}, Tb^{3+} and Ce^{3+}/Tb^{3+} doped zinc-sodium-aluminosilicate glasses, *Opt. Mater.*, 2012, **33**, 1892.

56 C. Zhang, T. Uchikoshi, R.-J. Xie, L. Liu, Y. Cho, Y. Sakka, N. Hirosaki and T. Sekiguchi, Reduced thermal degradation of the red-emitting $Sr_2Si_5N_8$:Eu^{2+} phosphor *via*

thermal treatment in nitrogen, *J. Mater. Chem. C*, 2015, **3**, 7642.

57 Y. J. Park, S. W. Kim, C. J. Kim, Y. J. Lee and J. Hwang, Development of β-SiAlON:Eu^{2+} phosphor in glass for high-power LED-and LD-based lighting systems using original BaO-B_2O_3-ZnO-SiO_2 (BBZS) composition glass, *J. Alloys Compd.*, 2019, **794**, 94.

58 Y. J. Park, G. J. Jeong, J. H. Kim, Y. Lee, S. W. Kim, C. J. Kim and J. Hwang, Development of high luminous efficacy red-emitting phosphor-in-glass for high-power LED lighting systems using our original low T_g and T_s glass, *Opt. Lett.*, 2019, **44**, 6057.

59 Y. Li, L. Hu, B. Yang, M. Shi and J. Zou, Effect of sintering temperature on the photoluminescence properties of red-emitting color conversion glass, *J. Mater. Sci.: Mater. Electron.*, 2018, **29**, 2035.

60 Y. K. Lee, Y. H. Kim, J. Heo, W. B. Im and W. J. Chung, Control of chromaticity by phosphor in glasses with low temperature sintered silicate glasses for LED applications, *Opt. Lett.*, 2014, **39**, 4084.

61 W. J. Chung and Y. H. Nam, A review on phosphor in glass as a high power LED color converter, *ECS J. Solid State Sci. Technol.*, 2019, **9**, 016010.

62 L.-Y. Chen, W.-C. Cheng, C.-C. Tsai, Y.-C. Huang, Y.-S. Lin and W.-H. Cheng, High-performance glass phosphor for white-light-emitting diodes *via* reduction of Si–Ce^{3+}:YAG inter-diffusion, *Opt. Mater. Express*, 2014, **4**, 121.

63 S. Oshio, T. Matsuoka, S. Tanaka and H. Kobayashi, Mechanism of Luminance Decrease in $BaMgAl_{10}O_{17}$:Eu^{2+} Phosphor by Oxidation, *J. Electrochem. Soc.*, 1998, **145**, 3903.

64 G. Bizarri and B. Moine, On $BaMgAl_{10}O_{17}$:Eu^{2+} phosphor degradation mechanism: thermal treatment effects, *J. Lumin.*, 2005, **113**, 199.